AmbiSense: Acoustic Field Based Blindspot-Free Proximity Detection and Bearing Estimation

Siddharth Rupavatharam†, Xiaoran Fan†, Caleb Escobedo,
Daewon Lee, Larry Jackel, Richard Howard, Colin Prepscius, Daniel Lee, and Volkan Isler

***Abstract*— In this paper, we present *AmbiSense*, an acoustic field based sensing system that performs proximity detection and bearing estimation for safer physical human-robot interactions. A single low cost piezoelectric transducer is used to setup this novel acoustic sensing modality to create a blindspot-free sound field engulfing a robot arm. Two detection algorithms leveraging spectral information from reflected audio waves of objects entering the acoustic field are proposed to infer object presence and bearing. We also present a new receiver structure which improves signal to noise ratio (SNR). *AmbiSense* is paired with a collision avoidance inverse kinematic solver for real world deployment on a Kinova Gen3 robot. Validation is performed using ten test objects generating 2000 proximity and bearing estimation events in real world settings, we show that *AmbiSense* detects proximity with 93.8% sensitivity and 96.6% specificity. It estimates bearing and maps it to three zones on a robot link with 100% sensitivity and specificity, while using fewer sensors than state of the art methods for similar coverage.**

I. Introduction

As more robots make their way into human work spaces to help assist and work collaboratively, unstructured and dynamic human environments pose a challenge for safe physical interactions. Robots therefore need to be able to sense their immediate surroundings to detect mobile humans and other objects in motion. Endowing robots with blindspot free, omni-directional sensing abilities improves awareness of their surroundings, helping them anticipate and avoid potentially dangerous collisions.

State of the art solutions leverage technologies such as capacitance, infrared, and acoustic sensing as well as cameras to detect objects that are physically close to the robot. Capacitive sensors deployed in a skin-like manner cover the entire surface of the robot, with commercial solutions such as the Bosch APAS deploying more than 120 individual sensing units [1]–[3]. While this achieves dense coverage and increases localization acuity, sensor deployment across the robot surface is expensive and complicated to perform. Retrofitting a robot surface requires modifications which may not be feasible due to complex surface topology. Furthermore, electric conductivity and dielectric constant of a wide range of objects are similar making sensing challenging. Other technologies such as infrared, mmWave, magnetic, and acoustic sensing utilize highly directional signals with narrow cones of sensing, restricting detection to fixed field of views [4]–[6]. Camera based techniques suffer occlusions from obstacles blocking their field of view and are sensitive to lighting conditions [7].

†Authors contributed equally to this work

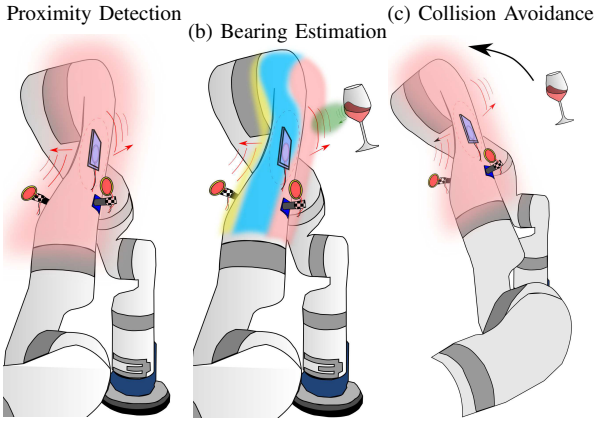

Fig. 1: *AmbiSense* system with (a) a piezoelectric transducer (in purple) vibrates the robot link to create an acoustic field around the entire link without blind spots (in red). Objects that enter the field reflect acoustic signals (in green). Two piezoelectric transducers attached to the novel acoustically isolating raised structure deployed on both sides of the robot link, sense changes in the acoustic field to detect proximity. (b) Robot detects object proximity and maps bearing to zones (in yellow, blue, and orange), a fourth side behind the blue zone, also considered a part of blue zone is not visible in this image. (c) Collision avoidance maneuver using bearing information input to an inverse kinematic solver.

These shortcomings hinder wider adoption of existing sensing technologies and elicit the need for occlusion resistant and field of view independent sensing systems. Along with sparse deployment of sensors with simple installation on any robot surface. In this paper, we present *AmbiSense*, an acoustic field based blindspot-free sensing system, that performs: (i) close range proximity detection of objects $\leq 25cm$ from the robot surface, and (ii) bearing estimation of the detected object. Bearing is defined as the direction of the object relative to the robot link as shown in Fig. 1. The proposed sensing system realizes these capabilities using a novel acoustic field sensing modality utilizing far fewer sensors and simpler installation compared to existing methods for similar coverage. Also, *AmbiSense* can be used standalone or in conjunction with existing sensing methods such as capacitive sensing.

AmbiSense utilizes the entire surface of a robot link to generate ultrasonic waves and form an encompassing acoustic field around the link. What it senses is the interference signal created by objects entering the field. Our study shows how these signals are used to infer proximity and bearing of the interfering objects. Sec. III discusses the setup, characteristics and salient features of this sensing modality in more detail.

To successfully realize *AmbiSense*, several hardware and software solutions are implemented overcoming challenges.

First, a novel mounting structure that physically raises the receiver from the surface while acoustically isolating it from noise on the surface is constructed. Reflected acoustic signals obtained by receivers mounted on the robot surface get drowned out by mechanical and electrical noise present on the surface. The relative magnitude of this noise while high on the surface, decreases away from the surface. The reflected acoustic signal varies with distance from the surface; by raising the receiver up from the surface an improved signal compared to noise can be obtained. Second, a narrow band coherent detection pipeline is used to extract information from the small reflected acoustic signals that occur in a large background signal. Unprocessed reflected signals received at the acoustically isolated receiver have amplitudes in μV. Third, we design light-weight proximity detection and bearing estimation algorithms that use spectral properties of the reflected acoustic signals. The proposed algorithms generalize well in detecting various everyday objects even when the robot moves in arbitrary trajectories.

In summary, the main contributions of this paper are:

- **Novel sensing modality:** Acoustic field based blindspot free sensing using fewer sensors with easy installation
- **Detection algorithms:** Proximity detection and bearing estimation algorithms that are lightweight, robust, and generalize well over arbitrary robot motion trajectories
- **Sensor design:** A novel receiver mounting structure that improves signal to noise ratio by acoustically isolating noisy vibrations from robot motion artifacts
- **Real world control:** Integrating processed sensor data with a collision avoidance inverse kinematic solver. A real-time system is prototyped on a Kinova Gen3 robot arm to demonstrate *AmbiSense*'s capabilities under several realistic settings.

II. Related Work

Navarro et. al. [8] define proximity range as distances $\leq 50cm$ from the robot surface. Sensing techniques used to perform proximity detection and bearing estimation in this range are discussed in this section.

1) Capacitive sensing: This sensing method utilizes electric fields to sense objects that are near the robot. Sensors made of metal plates emit an electric field and monitor changes in it as objects enter the field. Capacitive sensors deployed on robot surfaces have been to shown to perform object, distance, contour, and material detection, as well as estimate bearing [9]–[11]. Bearing is defined as determination of direction of an object relative to the robot [1], [2]. However, capacitive sensing systems find it challenging to sense a wide range of objects, as change in capacitance depends on the shape, orientation, electric conductivity, dielectric constant and object coupling to ground. Further, as each sensor emits an electric field over a limited area, the entire surface needs to be instrumented with an array of sensors as demonstrated by Bosch APAS [3]. While theoretically one large sensor with contours can be used to cover an entire robot surface, it would come at the expense of low localization resolution. Finally, deploying capacitive sensors requires heavily modifying the outside surface of the robot system, making integration hard and requiring bespoke sensors for different surface topologies.

2) Infrared and mmWave RADAR: Infrared Ranging (IR) and millimeter Wave Radio Detection And Ranging (mmWave RADAR) transmit electromagnetic radiation that reflects off objects. Object presence, distance, bearing, and velocity are calculated based on the properties of the reflected waves; such as changes in phase, amplitude or frequency. IR and mmWave sensors are highly directional and have fixed cones of sensing, requiring a large number of sensors to cover all areas around a robot. Some IR systems leverage this dense deployment across the robot surface to fuse information from multiple sensors to act as a unified distributed distance sensor [12]–[14]. Other solutions deploy mmWave RADAR sensors on robot surfaces [4], [15], [16] but do not fare well when objects are in close-proximity to the sensor.

3) Cameras: Camera based proximity and collision avoidance solutions have also been proposed [17], [18]. They are dependent on focal length, viewing angle, illumination conditions, and line of sight. Robots entering the camera's field of view may cause occlusions, making it challenging to detect objects in close proximity.

4) Acoustic sensing: Fan et al. [19] propose AuraSense, a sensing system that uses leaky surface waves to perform blind spot free collision avoidance. Their system uses a receiver that is attached directly to the surface of a robot, causing it to be susceptible to mechanical noise due to robot motor vibrations. The surface based receiver has poor signal to noise ration (SNR) and finds it challenging to detect acoustic field changes that occur above the robot surface. A 1D convolutional neural network is used to detect proximity which performs poorly in real world settings as the network model does not generalize well across different obstacles and robots, speeds of operation, and robot motion trajectories. It is also infeasible to collect a dataset that generalizes across all the mentioned variables. These challenges necessitate the need for receivers with better SNR and algorithms that generalize and perform well in real world settings.

Other approaches use piezoelectric transducers capable of generating pulses of ultrasonic sound $\geq$ 40 kHz that reflect off objects. The distance to an object and its position are determined based on the round trip time a pulse takes, making it challenging to sense objects close to the sensor [20]–[22]. Ultrasonic sensing systems deploy transmitter-receiver pairs that have fixed cones of sensing, requiring several sensors to cover all sides of a robot.

III. Acoustic field sensing

Acoustic fields as illustrated in Fig. 1 are regions where acoustic waves propagate freely without obstructions that would otherwise interfere with the sound path. The system as shown in Fig. 2 uses a piezoelectric transducer mounted onto the surface of a robot using a thermoplastic adhesive. The transducer is excited causing it to vibrate and transfer vibrations to the entire surface of the robot. These vibrations further spread into the air above the surface all around the

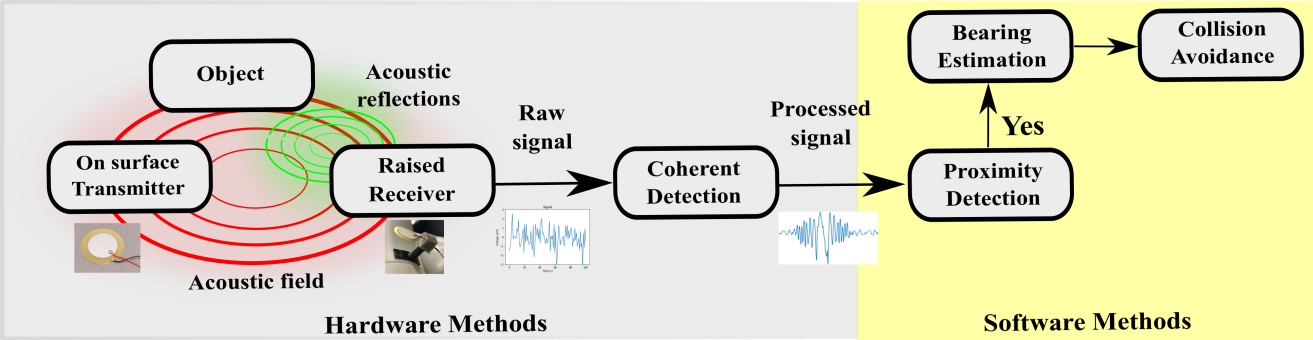

Fig. 2: *AmbiSense* proposes hardware and software contributions. It utilizes two independent transducers, to generate and receive reflected acoustic vibrations present above the surface. The raw received signal is multiplied with a copy of the original transmitted signal and low pass filtered. Proximity and bearing are inferred utilizing spectral information of the processed signal.

robot setting up an acoustic field. Objects that approach the robot surface and enter the acoustic field reflect sound waves back towards the surface which interfere with the existing sound waves in the acoustic field. This interference pattern contains information about the distance and bearing of the object. Transducers raised above the robot surface serve as receivers that sense changes in the acoustic field.

Acoustic field based sensing methods presented in Sec. IV are distinctive from conventional sensing methods in several ways: (i) the entire robot surface vibrates to generate an acoustic field in contrast to point source transmitters, assuring a continuous and wide sensing area, (ii) the interference pattern in the acoustic field diffracts around the surface, enabling multiple independent receivers to sense wider changes locally, (iii) potentially any surface stiff enough to vibrate can be used to generate an acoustic field and perform sensing, (iv) sensor deployment involves merely mounting transducers, therefore even surfaces with complex topologies can be instrumented without the overhead of requiring surface or sensor modifications, and (v) only a handful of sensors are required to create a wide acoustic field over a surface and perform sensing, compared to tens or hundreds required in various state-of-the-art solutions. These salient features put *AmbiSense* in a new class of acoustic aura based blind spot free detection systems.

IV. System Design

A. Proximity detection

Objects that enter and exit the acoustic field reflect sound waves creating interference in the field. As the receiver mounted on the robot is present in the acoustic field, it receives a large transmitted signal, the carrier, and a small interference signal, the envelope. The interference signal is present as undulations on the envelope of the received carrier signal. Therefore, the presence of undulations are indicative of proximity in an otherwise stable carrier signal. The envelope of the received signal is extracted using a narrow band coherent detector described in Sec. IV-D, which effectively removes the carrier signal. The amplitude and oscillations of the undulations provide information about the distance of the object from the robot. As an object moves closer to the robot, the number of oscillations decrease while the amplitude rises. Evaluation tests and field studies indicate that the extracted undulation signal is a function of object distance, shape, size, velocity of approach or departure, and material of an object. Objects of different sizes approaching the robot at the same velocity and angle produce undulations which have similar oscillations but different amplitudes. As detection of proximity depends on the amplitude and rate of oscillations of the undulation signal, an algorithm that leverages spectral information of a signal is proposed and described next.

The extracted envelope signal represented as $y(t)$, is processed in time windows α seconds in length. Spectral information $\mathcal{Y}_\alpha(\Omega)$ of each $y(t)_\alpha$ is obtained using the Fourier Transform,

$$\mathcal{Y}_\alpha(\Omega) = \int_{-\infty}^{\infty} y_\alpha(t) e^{-i2\pi\Omega t}\, dt, \quad \forall \Omega \in \mathbb{R}. \tag{1}$$

The Fourier Transform decomposes a time domain signal into its constituent frequency domain components with corresponding magnitudes. Hence, $\mathcal{Y}_\alpha(\Omega)$ is a vector of length n with each element being the magnitude of a frequency present in $y(t)_\alpha$. Spectral powers up to a frequency f_{max} are summed up to compute $\mathcal{P}$, which is compared to a threshold γ to determine whether an object is in proximity,

$$\mathcal{P} = \sum_{n=1}^{f_{max}} \mathcal{Y}_\alpha(\Omega_n), \tag{2}$$

$$\text{Proximity} = \begin{cases} 1, & \mathcal{P} > \gamma, \\ 0, & \text{otherwise.} \end{cases} \tag{3}$$

The algorithm therefore informs the system of a proximity event every α seconds.

Parameter value selection and algorithm evaluation are presented in Sec. V-A.3.

B. Bearing Estimation

Two receivers mounted at different locations on the robot sense the same undulations as described in Sec. IV-A but with different amplitudes. This is due to the acoustic field being continuous and non-uniform over the entire surface. The undulation signals that reach multiple receivers suffer from diffraction around the robot. It is observed that this diffraction affects their amplitude more than frequency and undulation signals detected by receivers closer to the object

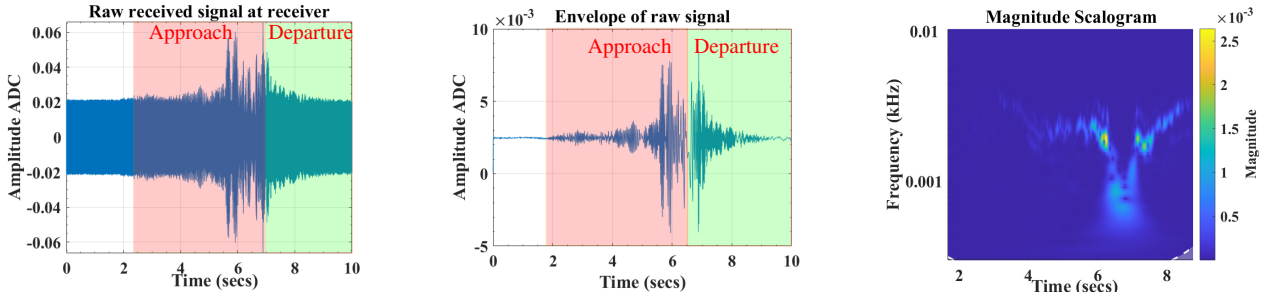

Fig. 3: (a) 46kHz raw received signal, dark blue parts are the transmitted signal. (0 - 2sec) no object in proximity, (3 - 4sec) objects starts approaching the robot and creating undulations in the envelope, (4 - 6sec) close proximity, (7 - 9sec) moving away, (b) extracted envelope post narrow band coherent detection, signal trace only contains perturbations and undulations related to object proximity, (c) only frequencies between 1 to 100 Hz are present in the extracted envelope, with lighter color signifying higher frequency magnitude.

tend to have higher amplitudes than receivers located far away. Additionally, amplitude of undulation signals arising from objects in between two receivers are similar. A spectral power based algorithm is proposed to uniquely demarcate the robot surface into zones as shown in Fig. 1. Bearing of the object is inferred based on the zone the detected object is closest to.

In order to identify the zone closest to the object, summed spectral power of signals from two receivers located on opposite sides of a robot link as shown in Fig. 1 are computed similar to Eq. 2 described earlier in Sec. IV-A. This generates a continuous stream of spectral data $\mathcal{P}_1$ and $\mathcal{P}_2$. By comparing these summed spectral values to zone specific thresholds object bearing is obtained.

$$\text{zones} = \begin{cases} 1, & \mathcal{P}_1 > \gamma_0 \quad \text{and} \quad \mathcal{P}_2 < \gamma_0, \\ 2, & \mathcal{P}_1 < \gamma_0 \quad \text{and} \quad \mathcal{P}_2 > \gamma_0, \\ 3, & \mathcal{P}_1 > \gamma_1 \quad \text{and} \quad \mathcal{P}_2 > \gamma_2, \end{cases} \tag{4}$$

values of α, f_{max} are unchanged from the proximity detection algorithm, while γ_0, γ_1, γ_2 are set based on a single robot specific calibration step. The algorithm therefore informs the system of an object bearing event every α seconds. Zones 1 and 2 have similar thresholds as the receivers are present in the zone, whereas Zone 3 has a receiver specific threshold. This is attributed to asymmetry in deployment giving rise to different distances to each receiver which affect signal amplitude.

Longitudinal and cross-sectional visualization of the zones are shown in Fig. 1 and Fig. 6c respectively.

C. Novel receiver mount design

AmbiSense uses an ultrasonic signal to excite a single Lead Zirconate Titanate (PZT) piezoelectric crystal transducer attached to the surface of the robot to create the acoustic field above the surface. As piezoelectric transduction works both ways, that is, mechanical vibrations produce electric charge and vice versa, another PZT crystal transducer is used as a receiver.

A significant part of the reflected and interference signals can be better obtained above the surface rather than on the surface as shown in Fig. 4. In order to improve the signal-to-noise ratio (SNR, we prototype the mount to have the receiver suspended in air. Keeping the receiver raised decouples it from the surface where noise is high and couples it with acoustic field where the signal is high, increasing SNR. A visualization of the raw received signals from the two different mounting configurations are shown in Fig. 4b and Fig. 4d. The amplitude of the received signal is the sum of the amplitudes of the transmitted wave, the reflected wave, and the noise launched from the surface. The percentage contribution of the reflected wave is higher for the above the surface receiver compared to the on the surface receiver, even if the overall amplitude is smaller.

The challenge lies in raising the receiver to have it hover in the air just above the robot surface, in a way that is easy and repeatable to deploy, maintains a fixed orientation, and is poorly acoustically coupled to the surface. This is accomplished by assembling a novel raised receiver as shown in Fig. 4a. A thin-walled, hollow cylinder of low-mass and minimal surface area in contact with the robot surface is designed and 3D printed to hold the transducer raised above the surface. This design reduces acoustic coupling to surface vibrations and limit noise from reaching the transducer through the structure holding it up. Structures with greater mass and larger contact surfaces acoustically couple and transfer vibrations readily. To further reduce noise, sound absorbing foam is added between the cylinder and transducer with wires originating from the transducer being passed through this foam. Sound absorbing foam helps dampen acoustic waves over a wide frequency range, attenuating any vibrations that travel up through the cylinder or along the wires connected to the transducer. The base of the cylinder is attached to the robot surface using off-the-shelf double sided sticky tape.

D. Coherent detection of acoustic signals

The raw received signal is a combination of of the transmitted wave, the reflected wave, and the noise launched from the surface. The transmitted wave is considered as the carrier wave on the envelope of which the reflected wave or interference signal is found, this is shown in Fig. 3a and Fig. 4b. The envelope of the signal contains information necessary to enable proximity detection and bearing estimation, and is extracted using coherent detection. Signal mixing is one way of performing coherent detection, where a received signal is

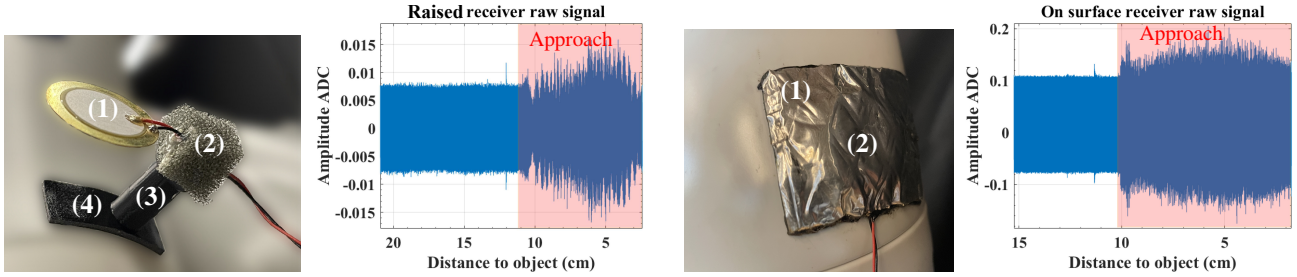

(a) (b) (c) (d)

Fig. 4: (a) (1) Piezoelectric transducer, (2) Sound absorbing foam, (3) Hollow cylinder, (4) Sticky tape , (b) Raw received signal of robot approaching a stationary object, undulations start from 11cm away shown in the red shaded region, (c) (1) Sound deadener covers the (2) piezoelectric transducer, (d) Raw received signal of robot approaching a stationary object, undulation amplitude is a smaller fraction of the total signal proximity signal, the envelope is noisy and undulations harder to see in the red shaded region.

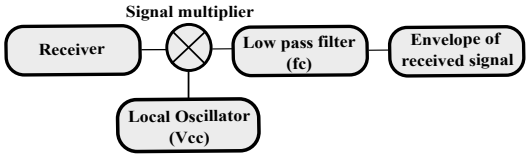

Fig. 5: Coherent detection using signal mixing: multiplying the received signal with a copy of the original transmitted demodulates information present at a higher frequency to a lower frequency. In *AmbiSense*, the received and transmitted signal frequencies are set to be equal, to demodulate the envelope of the high frequency received signal as a DC level change.

multiplied (i.e., mixed) with a copy of the transmitted signal to demodulate the information present in the received signal as frequency modulations [23], [24].

Signal mixing results in two signals,

$$y(t) = \underbrace{\frac{AB}{2}\cos(\phi_1 - \phi_2)}_{\text{DC}} - \underbrace{\frac{AB}{2}\cos(2\pi(2f)t + (\phi_1 + \phi_2))}_{\text{AC}}, \tag{5}$$

where, A and B are the received and transmitted signal amplitudes with corresponding phases ϕ_1 and ϕ_2. Given the transmitter and receiver share the same frequency, the first signal occurs at a frequency close to DC and the second at the sum of both frequencies. The second signal is filtered out using an appropriate low pass filter, leaving behind just the first signal corresponding to the interference as shown in Fig. 3b. The signal mixing schema is shown in Fig. 5.

E. Transmission frequency selection

A linear chirp signal, $f(t) = ct + f_0$ from 19 kHz to 200 kHz is used to excite the transducer to find a single suitable transmit frequency. Where, the chirp rate c is assumed constant with $c = (f_1 - f_0)/T$, f_0 is frequency at time $t = 0$, f_1 is final frequency, and T is the time it takes to sweep from f_0 to f_1. Voltage at the receiver transducer after coherent detection is measured and a spectrogram plot is used to find the frequency with the highest magnitude. 46 kHz is chosen as the excitation frequency.

F. Threshold value calibration

The transducer mounted on the surface is excited using a 15 V_{rms} 46kHz signal and the robot manipulator is programmed to move in an preset path without any objects in close-proximity. To determine the value of γ, $\mathcal{P}$ is computed for each receiver and averaged over 30 seconds (See Eq. 2). γ is set to this averaged value. The robot is then made to approach a fixed object using the side assigned to Zone 3 to compute γ_1 and γ_2 similar to γ.

G. Integration with CollisionIK

To demonstrate some possible real-world capabilities of our system to detect and react to dynamic objects in the environment we integrate our system with the CollisionIK per-pose inverse kinematic solver [25]. CollisionIK can be used to avoid objects near the robot in real-time by solving for joint positions that minimize multiple objective functions such as pose, self-collision, velocity, acceleration, and jerk [26].

V. Evaluation

Receiver mount design and proximity sensing range are evaluated first followed by proximity detection and bearing estimation performance in real world deployment scenarios. Real time collision avoidance performed by integrating proximity data with the Collision IK solver is discussed last. Two thousand proximity events were collected using the 10 objects shown in Fig. 7a for evaluation. A Kinova Gen3 is used for all experiments.

A. Sensor Evaluation

1) Receiver mount design: In this experiment, we explore different design factors that affect SNR based on Sec. IV-C. Specifically, we observed changes in SNR while varying the mount height and material. The results for stationary and dynamic conditions are shown in Table I.

SNR is calculated using,

$$\text{SNR} = 10\log_{10}\left[\frac{\text{M}_{signal}}{\sum_{i=1}^{n}\text{M}_\text{i}}\right], \forall\ i \neq signal, \tag{6}$$

where M_{signal} is the power spectrum magnitude of the transmit frequency and M_i are power spectrum magnitude of all other frequencies.

Receiver mounts are made using wooden dowels and Polylactic acid (PLA), as these materials are available off-the-shelf and mounts can reproducibly be crafted. While the wooden dowels are solid, the 3D printed PLA cylinders

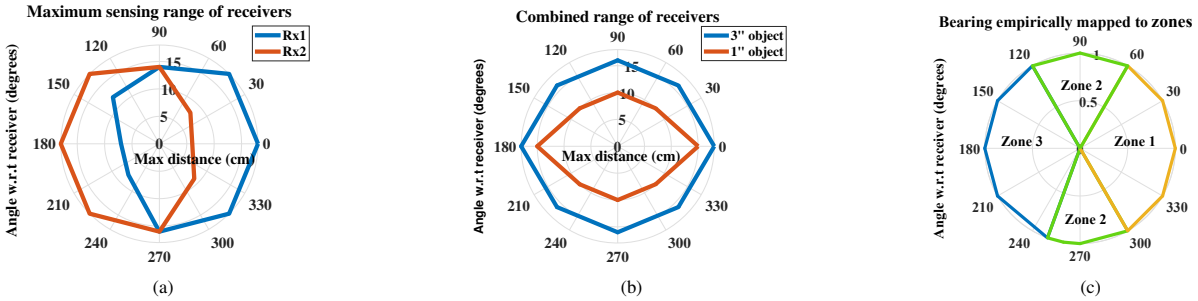

(a) (b) (c)

Fig. 6: (a) Sensing range of receivers, Rx1 faces right Rx2 faces left, (b) Sensing range as a function of object size, the 1" has to be closer to be detected and (c) Zones for bearing estimation around robot link, range normalized to 1.

TABLE I: Comparison of SNRs across different mount heights, materials, stationary and moving robot

Height	Stationary robot		Moving robot	
	Wood	PLA	Wood	PLA
10mm	13.5dB	22.1dB	12.2dB	21.4dB
15mm	6.2dB	20.7dB	5.3dB	18.7dB

TABLE II: Transducers required to cover a robot link ($17430mm^2$)

Authors	Transduction method	Transducers
AmbiSense	**Acoustic**	**3**
Bosch APAS [3], [27]	Capacitance	45
Cheng et al. [12]	Optical	800
Watanabe et al. [28], [29]	Optical	800

are hollow, with both cylinders having a diameter of 5mm. SNR at the receiver is calculated by collecting and averaging values over a period of several days, while a signal of 10 V_{rms} and 46 kHz is used to excite the transducer. We see that the raised receiver built using PLA demonstrates highest SNR consistently across trials. Results follow the intuition that materials such as hollow PLA cylinders having low-mass are poorer acoustic conducters compared to solid woodern dowels with higher mass.

2) Receiver sensing range: This subsection describes experiments used to find the maximum sensing range of our raised receivers. A hollow PVC pipe of outer diameter 2.5" and height 8" is used as a static object, towards which, the robot arm with raised receivers approaches using different sides of a link in steps of 45 degrees. Fifteen approaches are performed per robot link side, with values of f_{max} and α set to 100 Hz and 0.2 seconds respectively. γ is set using the calibration step described in Sec. IV-F. The process to obtain the maximum sensing range is as follows: First, the sensing signals are processed via the coherent detection pipeline. The processed signal is then passed to the proximity detection algorithm. Finally, we report the range values at which proximity is detected in Fig. 6a using polar coordinates.

Results show that receivers sense objects up to a range of 20 cm away for shallow approach angles, and 15 cm away for steeper angles. Further, Fig. 6a also shows that each receiver senses all around the robot and possesses 360 degree field of view without blind spots.

Sensing range as a function of object size: The same experiment as described earlier is performed, with PVC pipes 1" to 4" in diameter used as static objects instead. Values of γ, α and f_{max} are kept unchanged. Object size specific maximum distance is noted. Objects 3" across are detected up to 20 cm away for shallow approach angles, and 15cm away for steeper angles, whereas, 1" objects are detected up to 15 cm away for shallow approach angles, and 10cm away for steeper angles. Polar plots of sensing distance as function of object size and approach angle are shown in Fig. 6b.

Results show that larger objects reflect more of the acoustic waves back and are sensed from further away compared to smaller objects. *AmbiSense* detects objects of varying sizes approaching a robot link from all around and does not require parameter changes to detect different objects.

Number of sensors and coverage: A single robot link has a surface area of approximately $17430mm^2$. Table II shows a comparison of the required number of individual sensing units depending on sensing modality to cover this area without overlaps. Capacitance sensors have larger surface areas allowing for wider sensing, while optical sensors have directivity angles as narrow as 10° to 30° limiting sensing area.

3) Mapping zones uniquely based on receiver locations: As described in Sec. IV-B bearing of an object is estimated using received signal from two receivers. Objects closer to specific parts of the robot influence the spectral properties of reflected signals uniquely, enabling identification. The three mapped zones are shown in Fig. 6c, each zone roughly covering a third of the surface of the robot link. Sensing area of each Zone extends longitudinally as depicted in Fig. 1 with both receivers placed symmetrically and approximately towards the center of the robot link. The same experimental setup described earlier in Sec. V-A.2 is used with the robot arm made to approach a static PVC pipe. Summed spectral power $\mathcal{P}$, as described in Sec. IV-A is calculated per receiver and paired with object position to map out sensing zones.

Results show that the surface of the robot has three uniquely addressable zones when two receivers are used. There exists a degeneracy that occurs naturally within Zone 2, that is, front and back areas show similar $\mathcal{P}$ values on both receivers due to the symmetry in deployment. Information from an additional receiver is required to break the degeneracy and independently address the two areas in Zone 2 uniquely. However, receiver locations determine where the degeneracy and Zone 2 get mapped, giving system designers control over areas that can potentially tolerate the degeneracy. For example, a side that predominantly faces another robot

(a) (b) (c)

Fig. 7: (a) Objects used for field study; they have different dielectric constants, optical, magnetic and acoustic reflective properties, (b) Hand (i.e., object) near real robot with two receivers on a robot link, (c) 3D visualization of robot and nearby object (i.e., sphere) representation in RViz.

link, that is, the side behind the blue zone in Fig. 1 that is not visible. Further, robot state information such as joint angles can be used to confirm self detection.

B. Field Study

Experiments are performed using ten different test objects as shown in Fig. 7a to evaluate system performance in real world settings. These objects are chosen in particular to evaluate sensing different dielectric constants, light, and sound reflective properties of objects found in the real world. Experimental Data is collected across several weeks to take into account temperature, humidity, and other environmental variations.

1) Proximity detection: Each object is used to approach the robot arm 40 times for a duration of 1 sec. α is set to 0.2 seconds, the calibration step is performed to compute γ and 2000 real world on-robot object approach trials are recorded.

Two sets of tests are performed to evaluate proximity sensing capabilities, one with the robot arm being stationary and another with the arm moving in arbitrary trajectories. Test objects are brought close to the robot arm along different sides, using varied angles and approach speeds by a human experimenter, while ensuring no contact is made with the robot. Collected receiver signals are analyzed using the proximity detection algorithm discussed in Sec. IV-A. Results show 100% true positive rate (TPR) and true negative rate (TNR) when the robot is stationary. Zero false positives are reported, demonstrating proximity is only detected in the presence of objects and zero false negatives are reported, demonstrating only approaches involving objects are detected. When the robot is in motion, a TPR of 93.8% and TNR of 96.6% are obtained. Results show that the system is robust against false positives from surface vibrations and robot motion. Objects approaching in steep angles exposing lower surface area towards the robot are challenging to detect, as they reflect audio waves less, leading to false negatives. All observed false positives were due to robot self detections.

2) Bearing estimation: Similar to before, two sets of experiments are performed with the robot arm being stationary and mobile, and a human experimenter approaching the robot with test objects from different sides, angles and approach speeds. Collected receiver signals are analyzed using the bearing estimation algorithm. Results show 100% TPR and TNR of bearing estimation for each zone when the robot is stationary. This demonstrates that objects in close-proximity to the robot are mapped to their closest zones.

3) Control Example: Proximity and bearing estimation information from *AmbiSense* are used to avoid collisions in a dynamic physical human-robot interaction scenario. This example scenario is shown in fig. 7b and fig. 7c. CollisionIK a per-pose inverse kinematic solver is used to optimize for a particular end-effector pose while maintaining a separation distance between the robot and objects detected in the environment [25]. An additional objective term is added to the IK solver that favors the starting joint positions and moves the robot joint angles towards the favored positions when the object is removed from the scene. This control example is shown in the accompanying video. In this example, the robot is tasked to follow a predefined trajectory. When an object is detected in close proximity a virtual representation of the object is created to let the IK solver incorporate the avoidance objective. The IK solver is able to incorporate sensor data into the IK solving loop in real-time, demonstrating *AmbiSense* can be used in real robot systems to improve safety.

VI. Discussion

This section discusses observations from experiments and future work. An immediate following study will be performed to characterize acoustic fields and wave propagation as a function of voltage and frequency driving the transducer, surface material properties and topology. Existence of acoustic fields depend on the surface beneath receiving and propagating vibrations. These vibrations may not couple or propagate to a neighbouring link due to discontinuities in robot construction at joints, isolating surface vibrations to individual robot links and requiring each link to be excited independently.

False positives when a robot is in motion arise due to the robot detecting itself as an object, not due to detecting nonexistent objects. This can be mitigated using different acoustic frequencies on adjacent links combined with robot joint position information. Objects like wool, soft cloth, rubber, and sound absorbing foam are harder to detect as they absorb and dampen vibrations. Such objects can potentially be detected using higher relative speeds between robots and objects, exciting the transducer with a higher voltage, or altering approach angles. Additionally, the new raised receivers stick out like antennae and are susceptible to direct collisions.

Direct impact on the receiver may modify their directivity and sensitivity. An enclosure to protect the receivers without affecting sensing capabilities can be designed, which we leave for future work.

VII. Conclusion

In this paper, we present *AmbiSense*, an acoustic field based blindspot-free sensing system, that enables robots to sense proximity and bearing of objects in close vicinity. Our system realizes a novel sensing modality; acoustic field sensing generated using just one low cost ($\leq$ \$2) piezoelectric transducer. Object presence and bearing are inferred using two detection algorithms that leverage spectral information of interference in the acoustic field arising due to reflected audio waves. We also design a new receiver structure that improves signal to noise ratio (SNR) while discussing approaches to reduce vibrational noise transfer. This high SNR signal is processed using a narrow band coherent detector to extract information from reflections occurring in the acoustic field. Additionnally, *AmbiSense* is paired with a collision avoidance inverse kinematic solver and deployed on a Kinova Gen3 robot to show real-time collision avoidance. Validation using ten test objects that generate 2000 proximity and bearing estimation events in real world settings shows that *AmbiSense* detects proximity with 93.8% sensitivity and 96.6% specificity. It estimates bearing and maps it to three zones on a robot link with 100% sensitivity and specificity. Our experiments demonstrate *AmbiSense*'s potential as a generalizable, blindspot-free proximity sensing solution toward safe physical human-robot interactions.

References

[1] S. Tsuji and T. Kohama, "Sensor module combining time-of-flight with self-capacitance proximity and tactile sensors for robot," *IEEE Sensors Journal 2021*.

[2] A. Hoffmann, A. Poeppel, A. Schierl, and W. Reif, "Environment-aware proximity detection with capacitive sensors for human-robot-interaction," in *IEEE IROS 2016*.

[3] "APAS - Intelligent systems for human-robot collaboration APAS ASSISTAN CONTACT-FREE HUMAN-ROBOT COLLABORATION," https://www.lsa-control.com/pub/media/pdf/IoT/Apas.pdf, 2023, [Online; accessed 02-February-2023].

[4] C. Stetco, B. Ubezio, S. Mühlbacher-Karrer, and H. Zangl, "Radar sensors in collaborative robotics: Fast simulation and experimental validation," in *ICRA 2020*.

[5] S. Chang, Y. Zhang, F. Zhang, X. Zhao, S. Huang, Z. Feng, and Z. Wei, "Spatial attention fusion for obstacle detection using mmwave radar and vision sensor," *Sensors 2020*.

[6] Z. Flintoff, B. Johnston, and M. Liarokapis, "Single-grasp, model-free object classification using a hyper-adaptive hand, google soli, and tactile sensors," in *IEEE IROS 2018*.

[7] N. Garnett, S. Silberstein, S. Oron, E. Fetaya, U. Verner, A. Ayash, V. Goldner, R. Cohen, K. Horn, and D. Levi, "Real-time category-based and general obstacle detection for autonomous driving," in *ICCV Workshops 2017*.

[8] S. E. Navarro, S. Mühlbacher-Karrer, H. Alagi, H. Zangl, K. Koyama, B. Hein, C. Duriez, and J. R. Smith, "Proximity perception in human-centered robotics: A survey on sensing systems and applications," *IEEE T-RO 2021*.

[9] S. E. Navarro, S. Koch, and B. Hein, "3d contour following for a cylindrical end-effector using capacitive proximity sensors," in *IEEE IROS 2016*.

[10] T. D. Nguyen, T. Kim, J. Noh, H. Phung, G. Kang, and H. R. Choi, "Skin-type proximity sensor by using the change of electromagnetic field," *IEEE Transactions on Industrial Electronics*, 2020.

[11] Y. Ding, H. Zhang, and U. Thomas, "Capacitive proximity sensor skin for contactless material detection," in *IEEE IROS 2018*.

[12] G. Cheng, E. Dean-Leon, F. Bergner, J. R. G. Olvera, Q. Leboutet, and P. Mittendorfer, "A comprehensive realization of robot skin: Sensors, sensing, control, and applications," *Proceedings of the IEEE*, 2019.

[13] G. B. Avanzini, N. M. Ceriani, A. M. Zanchettin, P. Rocco, and L. Bascetta, "Safety control of industrial robots based on a distributed distance sensor," *IEEE Transactions on Control Systems Technology*, 2014.

[14] C. Escobedo, M. Strong, M. West, A. Aramburu, and A. Roncone, "Contact anticipation for physical human–robot interaction with robotic manipulators using onboard proximity sensors," in *IEEE IROS 2021*.

[15] S. Hazra and A. Santra, "Robust gesture recognition using millimetric-wave radar system," *IEEE sensors letters 2018*.

[16] C. Schöffmann, B. Ubezio, C. Böhm, S. Mühlbacher-Karrer, and H. Zangl, "Virtual radar: Real-time millimeter-wave radar sensor simulation for perception-driven robotics," *IEEE RA-L*, vol. 6, no. 3, pp. 4704–4711, 2021.

[17] H. Alvarez, L. M. Paz, J. Sturm, and D. Cremers, "Collision avoidance for quadrotors with a monocular camera," in *Experimental Robotics, Springer 2016*.

[18] G. Chen, W. Dong, X. Sheng, X. Zhu, and H. Ding, "Bio-inspired obstacle avoidance for flying robots with active sensing," *arXiv preprint*, 2020.

[19] X. Fan, R. Simmons-Edler, D. Lee, L. Jackel, R. Howard, and D. Lee, "Aurasense: Robot collision avoidance by full surface proximity detection," in *IEEE IROS 2021*.

[20] M. Toa and A. Whitehead, "Ultrasonic sensing basics," *Dallas: Texas Instruments*, 2020.

[21] Z. Tong, H. Hu, Z. Wu, S. Xie, G. Chen, S. Zhang, L. Lou, and H. Liu, "An ultrasonic proximity sensing skin for robot safety control by using piezoelectric micromachined ultrasonic transducers (pmuts)," *IEEE Sensors Journal 2021*.

[22] X. Fan, D. Lee, Y. Chen, C. Prepscius, V. Isler, L. Jackel, H. S. Seung, and D. Lee, "Acoustic collision detection and localization for robot manipulators," in *IEEE IROS 2020*.

[23] "The basics of mixers," accessed: 2022-08-29. [Online]. Available: https://www.digikey.com/en/articles/the-basics-of-mixers

[24] "Introduction to mixers," accessed: 2022-08-29. [Online]. Available: https://michaelgellis.tripod.com/mixersin.html

[25] D. Rakita, H. Shi, B. Mutlu, and M. Gleicher, "Collisionik: A per-instant pose optimization method for generating robot motions with environment collision avoidance," in *IEEE ICRA 2021*.

[26] C. Escobedo, N. Nechyporenko, S. Kadekodi, and A. Roncone, "A framework for the systematic evaluation of obstacle avoidance and object-aware controllers," in *IEEE IROS 2022*. IEEE, 2022.

[27] "APAS assistant Your flexible production assistant," http://robotforum.ru/assets/files/Bosch_pdf/boasch_apasassistant.pdf/, 2023, [Online; accessed 02-February-2023].

[28] K. Watanabe, M. Strong, M. West, C. Escobedo, A. Aramburu, K. C. Kodur, and A. Roncone, "Self-contained kinematic calibration of a novel whole-body artificial skin for human-robot collaboration," in *IEEE IROS 2021*. IEEE, 2021, pp. 1778–1785.

[29] VL53L1X, "Adafruit VL53L1X," https://learn.adafruit.com/adafruit-vl53l1x, [Online; accessed 25-February-2023].